Published as: H.J. Kuijf, J. de Bresser, M.I. Geerlings, M. Conijn, M.A. Viergever, G.J. Biessels, K.L. Vincken, "Efficient detection of cerebral microbleeds on 7.0T MR images using the radial symmetry transform", *NeuroImage*, 2012, nr. 3, vol. 59, pp. 2266-2273, DOI: 10.1016/j.neuroimage.2011.09.061.

Efficient detection of cerebral microbleeds on 7.0 T MR images using the radial symmetry transform

Abstract

Cerebral microbleeds (CMBs) are commonly detected on MRI and have recently received an increased interest, because they are associated with vascular disease and dementia. Identification and rating of CMBs on MRI images may be facilitated by semi-automatic detection, particularly on high resolution images acquired at high field strength. For these images, visual rating is time-consuming and has limited reproducibility. We present the radial symmetry transform (RST) as an efficient method for semi-automated CMB detection on 7.0 T MR images, with a high sensitivity and a low number of false positives that have to be censored manually.

The RST was computed on both echoes of a dual-echo T2*-weighted gradient echo 7.0 T MR sequence in 18 participants from the Second Manifestations of ARTerial disease (SMART) study. Potential CMBs were identified by combining the output of the transform on both echoes. Each potential CMB identified through the RST was visually checked by two raters to identify probable CMBs. The scoring time needed to manually reject false positives was recorded.

The sensitivity of 71.2 % is higher than that of individual human raters on 7.0 T scans and the required human rater time is reduced from 30 to 2 min per scan on average. The RST outperforms published semi-automated methods in terms of either a higher sensitivity or less false positives, and requires much less human rater time.

1 Introduction

Interest in cerebral microbleeds (CMBs) is increasing rapidly since a few years. CMBs are seen as phenomena distinct from larger haemorrhages. CMBs are associated with hypertensive vasculopathy, white matter hyperintensities and lacunar infarcts, and they are a key MRI marker of cerebral amyloid angiopathy (Greenberg et al. 2009; Knudsen et al. 2001; Theysohn et al. 2011; Vernooij et al. 2008; Wardlaw et al. 2006). CMBs consist of hemosiderin deposits (Fazekas et al. 1999) that are paramagnetic and cause a local susceptibility effect inside the magnetic field of the MR scanner. As a result, CMBs can be visualized as

round, hypointense spots on a T2*-weighted gradient echo MR sequence. At regular field strength (1 to 3 T), CMBs are usually defined as having a diameter ranging from 2 to 10 mm (Cordonnier et al. 2007).

The current standard for microbleed detection is visual rating with validated visual rating scales (Greenberg et al. 2009; Gregoire et al. 2009). As visual rating is time-consuming and has limited reproducibility, (semi-)automated detection may improve rating quality and decrease rating time. Recently, two methods on semi-automatic detection of CMBs have been published by Seghier et al. (2011) and Barnes et al. (2011). Seghier et al. described a method using a unified segmentation-normalization approach to detect microbleeds. The method identified 77 % of patients with microbleeds; no results were given on detection of the actual individual microbleeds. While numbers of false positives were not reported, manual removal of the false positives required 5 to 10 min on average. Barnes et al. used a combination of statistical thresholding and a support vector machine supervised learning classifier on susceptibility weighted images. This method detected 81.7 % of all individual microbleeds present in their data (identifying all patients). On average, over 100 false positives were found per patient, which takes a human rater 5 to 15 min to remove.

With the introduction of high-field 7.0 T MR scanners, detection of much smaller CMBs has become feasible (Conijn et al. 2010; De Reuck et al. 2011). However, while visual rating may be suitable for scans acquired at regular field strength, it takes a single rater about 30 min to assess a high resolution 7.0 T MR scan (typically $570 \times 570 \times 333$ voxels) for the presence of CMBs. This is due to the higher number of slices, the smaller size of the CMBs, and the fact that structures other than CMBs, in particular blood vessels, also show up at higher field strength. In a proof-of-principle experiment preceding this study, promising results have been published showing a large reduction in rating time when using the radial symmetry transform (RST) for semi-automatic microbleed detection (Kuijf et al. 2011). Moreover, an automated method might improve the accuracy of microbleed rating on 7.0 T MR scans. This is important, because it was observed that the inter-rater accuracy of visual rating of CMBs by experienced raters dropped from an ICC of 0.95 on 1.5 T MR scans to an ICC of 0.46 on 7.0 T MR scans (de Bresser et al. 2013). This is mainly due to reduced sensitivity, because CMBs on 7.0 T scans are easily missed by the human eye.

The goal of the present study was to develop a system with a high sensitivity, while minimizing the number of false positives, that provides automated detection of potential CMBs in a representative group of participants, and enables time-efficient visual censoring of false positive CMBs.

2 Methods and materials

Participants

For this study, 18 participants (mean age: 60 years, sd: 13 years, 15 men and 3 women) with microbleeds were included from the Second Manifestations of ARTerial disease (SMART) study (Simons et al. 1999). The objectives of the SMART study are to determine the prevalence of vascular risk factors and concomitant arterial disease and to study the incidence of future cardiovascular events and its predictors in patients newly referred to our hospital with

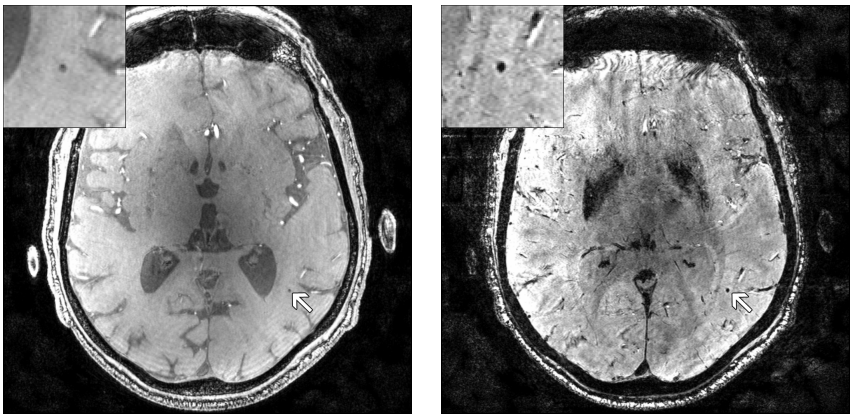

(a) First echo (b) Second echo

Figure 1: A typical slice of a 7.0 T T2*-weighted MR scan, showing the first and second echo. The arrows annotate a microbleed (enlarged in the upper-left corner).

atherosclerotic disease. The SMART study and the 7.0 T imaging were approved by the Medical Ethics Committee. Written informed consent was given by all participants. Of the 18 participants, 6 were included with diabetes mellitus, 4 with cerebrovascular disease, 2 with coronary artery disease, 2 with peripheral artery disease, 1 with hypertension, and 3 with other vascular risk factors or disease.

MRI acquisition

MRI acquisition was performed as described previously by Conijn et al. (2010), on a 7.0 T whole-body system (Philips Healthcare, Cleveland, OH). A dual echo T2*-weighted sequence was acquired (first echo time: 2.5 ms, second echo time: 15.0 ms, repetition time: 20.0 ms). A flyback gradient was applied between the first and second readout. Sensitivity encoding (SENSE) was applied in the RL direction. The images were reconstructed to $0.35 \times 0.35 \times 0.3$ mm^3 voxels and the built-in phase correction, partial-echo filter and homogeneity correction of the MR system were applied during reconstruction. A typical transversal slice of a high-resolution 7.0 T scan is shown in Figure 1.

Within the same scanning session, a 3D T1-weighted turbo field echo MR sequence was acquired, with a repetition time of 7.0 ms and an echo time of 3.0 ms. This scan was reconstructed to $0.66 \times 0.66 \times 0.7$ mm^3 voxels and SENSE was applied in the RL direction. This scan was used for preprocessing (see §2).

Visual rating of microbleeds

All scans were independently and visually scored by two raters, both neuroradiologists with more than 20 years of experience, as part of a previous study by Conijn et al. (2011). Minimal intensity projection post-processing of both echo times were presented simultaneously. The raters were blinded to all other clinical information. Rating of the microbleeds was performed according to

the Microbleed Anatomical Rating Scale (MARS), as described by Gregoire et al. (2009). In this rating scale, microbleeds can be defined as 'definite' or 'possible' microbleeds. A slight adjustment was made to the MARS by excluding the size-criterion. Owing to the blooming effect (McAuley et al. 2011), microbleeds appear larger on a T2*-weighted scan than the actual volume of the hemosiderin deposit. Therefore, a size criterion is ambiguous as microbleed sizes will vary among different scan sequences and parameter settings. For instance, increasing the echo time will increase the apparent size of the microbleeds on the T2*-weighted scan.

On T2*-weighted images, definite microbleeds were defined as black, round lesions on the first or second echo image. If such lesions were visible on the first echo, but were not larger on the second echo, they were not scored as microbleeds, for lack of a blooming effect by the longer echo time. If a rater was uncertain about a lesion being a microbleed, it could be rated as a possible microbleed. The lesions on which the two raters disagreed were evaluated in a consensus meeting to obtain a final score, containing definite and possible microbleeds.

In total, 54 microbleeds were visually detected in the 18 participants: 45 definite and 9 possible microbleeds. Of those microbleeds, 25 were detected by both raters, 9 only by rater 1, 19 only by rater 2, and 1 microbleed was initially not detected by one of the raters, but accidentally found during the consensus meeting. Both raters found additional lesions that were rejected as microbleeds during the consensus meeting: 4 were found by rater 1 and 18 by rater 2.

Preprocessing

The first two steps in the proposed method are the creation of a binary mask containing the grey and white matter, and intensity normalization. A probabilistic grey and white matter mask was generated from the T1-weighted sequence, using unified segmentation as implemented in SPM8 (Ashburner et al. 2005). The T1-weighted sequence was registered to the first echo of the T2*-weighted sequence and the resulting transform was applied to the probabilistic mask. A binary mask was created by thresholding the probabilistic mask at a level of 90 %. An example is shown in Figure 2.

The intensity values of the T2*-weighted scans were normalized to a range of [0, 255], using the 5th and 95th percentile of the histogram within the mask as lower and upper bound respectively. This standardized the grey values among different scans and will map the centre of visible microbleeds to a grey value of zero.

Radial symmetry transform

For the automatic detection of microbleeds, a 3D version of the original RST described by Loy et al. (2003) was implemented. The RST is a technique that utilizes local radial symmetry to highlight spherical points of interest in an image.

The choice for the RST is derived from the properties and shape of a CMB on the T2*-weighted MR sequence. The actual hemosiderin deposit is very small and accumulated in one point, as shown in histopathological research of Fazekas et al. (1999) and De Reuck et al. (2011), so it is safe to assume that

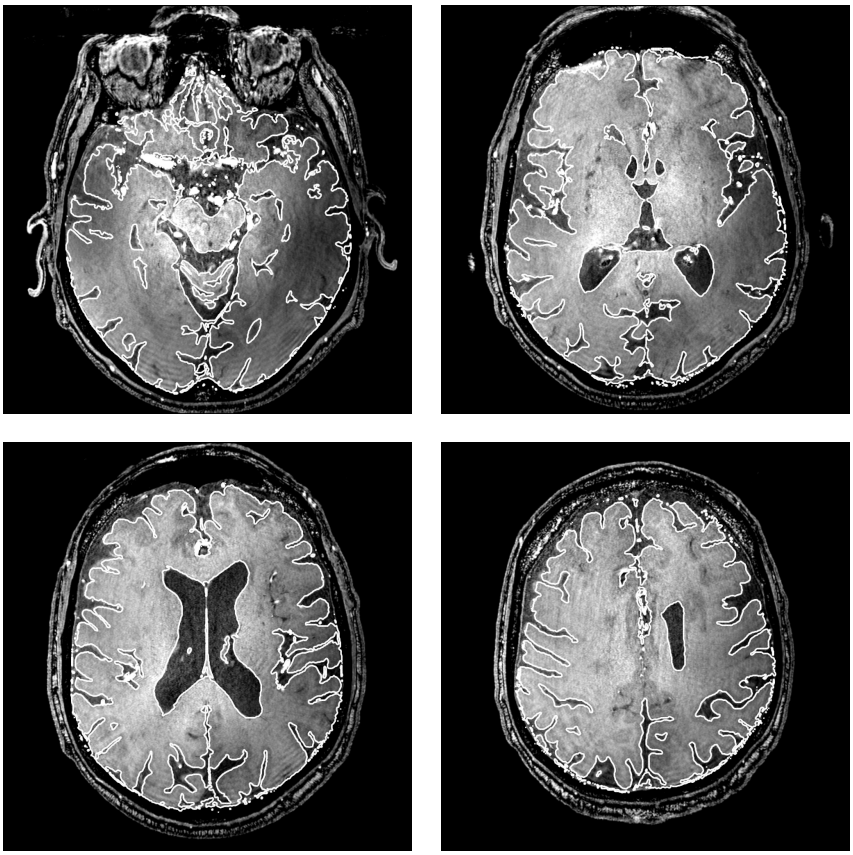

Figure 2: Example of the binary mask created during preprocessing, where the white contour indicates the boundaries of the binary mask.

the hemosiderin deposit is contained within a single voxel of the MR scan. The blooming effect of the microbleed, influenced by the echo time, is of approximately equal strength in all directions, which creates a spherical hypointense spot in the scan at the location of the microbleed. This fits perfectly into the concept of the RST.

The transform is computed for all radii $n \in N$, where N is a set of radii of microbleeds that need to be detected. In this study, the radii of CMBs to be detected ranged from 0.3 to 2.0 mm (step size of 0.1 mm), corresponding to the range of CMB radii that were detected by the raters.

Image gradients and orientations are used by the transform to infer the centre of mass of spherical objects in the scan, corresponding to potential microbleeds. The output value at a specific point of the transform with radius n indicates the contribution to the radial symmetry of the gradients a distance n from that point. The gradient information is computed using a fast 3D Sobel kernel of size $3 \times 3 \times 3$ voxels, giving positive values if the gradient direction points from dark to light. Since microbleeds are hypointense, the gradient direction information needs to be negated to have the gradient pointing towards the centre of the microbleeds. This is called 'negatively-affected' in the original

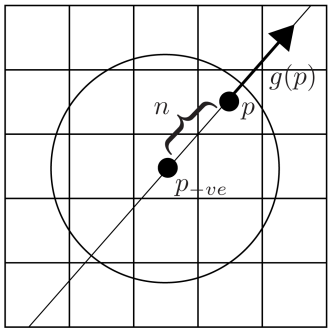

Figure 3: Given point p, the negatively-affected voxel p_{-ve} is found by following the gradient direction $g(p)$ in the opposite direction for some length $n \in N$. This process is repeated for all relevant gradients (controlled by β, see text) in the input image.

method by Loy et al. (2003).

At each radius $n \in N$, an orientation projection image O_n and a magnitude projection image M_n are computed, counting only negatively-affected voxels. The coordinates of a negatively-affected voxel p_{-ve} are given by

$$p_{-ve}(p) = p - \text{ round} \left(\frac{g(p)}{||g(p)||} n \right),$$

where p is a vector with the coordinates of the current voxel, g is the gradient and 'round' rounds each vector element to the nearest integer value. This is illustrated in Figure 3.

The orientation and magnitude projection images were initialized at zero. For each voxel p in the input image, the value at the corresponding point p_{-ve} in O_n and M_n was decremented by 1 and $||g(p)||$, respectively[1]:

$$O_n(p_{-ve}(p)) = O_n(p_{-ve}(p)) - 1,$$

$$M_n(p_{-ve}(p)) = M_n(p_{-ve}(p)) - ||g(p)||.$$

For a specific CMB with some radius n, each gradient on the surface of the CMB will map to the centre of that CMB, resulting in a local extreme in O_n, indicating the location of the centre of the CMB. As suggested by Loy et al. (2003), small gradients should be ignored during the computation of O_n and M_n. To this end, a parameter β was introduced as lower bound and set to 7.5 % of the highest gradient magnitude present in the image. This value was found during the preceding proof-of-principle experiment and eliminates noise and small variations in the scan that do not correspond to microbleeds.

The radial symmetry contribution of a single radius $n \in N$ is given by the convolution

$$S_n = F_n * A_n,$$

[1]Only negatively-affected voxels were taken into account here, whereas the original method also considers positively-affected voxels. Positively-affected voxels are ignored, as they correspond to hyper-intense spots.

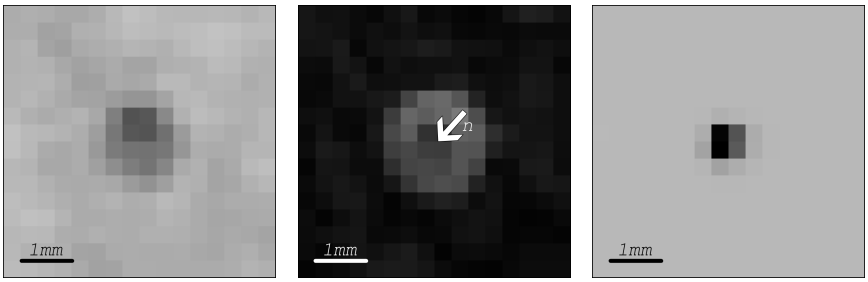

(a) CMB (b) Sobel operator (c) RST output

Figure 4: Output of the Sobel operator and the RST on the first echo of the microbleed, as shown in Figure 1. The n in 4(b) shows a possible radius from the set N. When using smaller or larger n, the radial symmetry contribution does not sum up in a single voxel.

where

$$F_n(p) = \frac{M_n(p)}{k_n} \left(\frac{|\tilde{O}_n(p)|}{k_n} \right)^{\alpha}$$

and

$$\tilde{O}_n(p) = \begin{cases} O_n(p) & \text{if } -k_n < O_n(p) \\ -k_n & \text{otherwise.} \end{cases}$$

In this equation, A_n was a 3D Gaussian used to smooth the output of the transform. The properties of this Gaussian were described by Loy et al. (2003) and is adjusted for each n as suggested. The used α is the radial strictness parameter, defining how strictly spherical the transform must be to return a high value. Its value was taken from our preceding proof-of-principle experiment (Kuijf et al. 2011), in which the optimal settings were investigated, and was set to 3. The parameter k_n is a scaling factor used to normalize O_n and M_n across different radii. When the radius increases, the number of gradient elements that can affect a voxel will also increase, since this can reach the number of voxels on the surface of the microbleed. The value for k_n was estimated empirically, as suggested by Loy et al. (2003), by inspecting the minimum value of O_n at microbleed locations. An expected minimum value of O_n was determined at each radius $n \in N$.

The resulting transform was computed as the sum over all radial symmetry contributions: $S = \sum_{n \in N} S_n$. The transform was computed separately per echo, resulting in an output for the first echo ($S1$) and the second echo ($S2$). Computation of the RST was performed on the whole scan and the result was masked afterwards with the grey and white matter mask obtained during preprocessing. An example output for a typical microbleed is shown in Figure 4.

As a final step, $S1$ and $S2$ had to be combined to generate a list of microbleed locations. Non-minimum suppression within a 2 mm neighbourhood was applied on both $S1$ and $S2$ to remove multiple minima close to each other. An upper-threshold was determined to extract the minima in S that might correspond to microbleeds. Separate upper-thresholds θ_1 and θ_2 were applied to $S1$ and $S2$, which were set at -20 and -100, respectively. These thresholds

were different from the preceding proof-of-principle experiment, partly because we extended the set of input scans on which the thresholds were determined heuristically and partly because the set of radii N differed. If within a 26-voxel neighbourhood around a minimum in $S1$ a minimum in $S2$ exists, this location is considered a potential microbleed. Finally, if the normalized grey value at the second echo of a potential microbleed was not equal to zero, it was removed from the list, since a microbleed should cause a signal void on the T2*-weighted images.

Experiments

In the experiments that were performed, the number of false positives present in the results was assessed together with the time to visually censor the false positives. A dedicated tool for this was developed using MeVisLab (MeVis Medical Solutions AG, Bremen, Germany). Two raters, rater 3 and 4, who were not involved in the original visual rating to ensure that they were not biased, each censored all potential CMBs identified by the RST. A consensus meeting was held for the cases on which the two raters disagreed.

When CMBs were detected by the RST that were not present in the original visual rating, they were added to the ground truth if raters 3 and 4 had confirmed them as true microbleeds. Adding the CMBs confirmed by raters 3 and 4 improved the ground truth rating and gave a fair comparison of the sensitivities of human raters versus the RST.

3 Results

The implemented 3D RST algorithm detected in total 353 potential microbleed locations in the 18 participants, on average 19.6 ± 12.1 (mean $\pm$ sd) microbleeds per participant. Among these locations, 35 true positives (present in the original visual rating) were found, 309 false positives, and 12 extra positives that were not present in the original visual rating, but were marked as potential CMB by the RST and confirmed by raters 3 and 4. Rater 3 required 43 min to censor all detected microbleeds (2.5 ± 1.5 min per participant; 7.9 ± 3.3 s per detected location), rater 4 28 min (1.5 ± 1 min per participant; 5.1 ± 2.2 s per detected location). Computation of the RST took about one hour per participant, using one core of a standard workstation.

In total, 66 microbleeds were detected (54 in the original visual rating after consensus, 12 extra positives were found by the RST), of which 34 were detected by rater 1, 44 by rater 2, 53 by both raters, and 47 by the RST (see Table 1). The single microbleed found only during the consensus meeting was not taken into account.

Sensitivities of the individual raters and the automatic detection are reported in Table 2. The RST had a sensitivity of 71.2 %, and the individual observers had a sensitivity of 51.5 % (rater 1) and 66.7 % (rater 2). The rating after the consensus meeting of raters 1 and 2 had a sensitivity of 80.3 %.

Some typical examples of the method, including true positives, false positives, and false negatives are shown in Figures 5–8. Figure 5 shows a typical microbleed present in one of the participants, which is detected by the RST. Another true positive is shown in Figure 6, where the CMB is adjacent to a

Table 1: **Upper part:** overview of the microbleeds detected during visual rating. **Middle part:** overview of the microbleeds detected by the RST. **Bottom part:** final overview of all detected microbleeds.

Participant:	1	2	3	4	5	6	7	8	9	10	11	12	13	14	15	16	17	18	
Visual[a]	Number of microbleeds detected																		Total
R1&R2	2	0	0	1	0	2	0	0	0	0	10	0	4	2	1	1	1	1	25
R1	1	0	0	0	0	0	0	0	3	0	2	0	0	0	0	0	2	1	9
R2	1	2	1	0	1	0	1	2	0	1	3	1	1	1	4	0	0	0	19
C	0	0	0	0	0	0	0	0	1	0	0	0	0	0	0	0	0	0	1
Total (VT)	4	2	1	1	1	2	1	2	4	1	15	1	5	3	5	1	3	2	54
Automatic[b]	Number of locations found																		Total
Total	20	47	13	24	21	30	8	11	27	36	18	7	11	37	18	16	3	6	353
TP	2	2	1	1	1	0	1	2	3	1	9	1	5	3	2	0	1	0	35
EP	1	0	0	0	0	4	0	0	1	0	1	0	1	0	1	0	1	2	12
FP	17	45	12	23	20	26	7	9	23	35	8	6	5	34	15	16	1	4	306
Final[c]	Number of microbleeds																		Total
VT+EP	5	2	1	1	1	6	1	2	5	1	16	1	6	3	6	1	4	4	66
FN	2	0	0	0	0	2	0	0	1	0	6	0	0	0	3	1	2	2	19

[a] R1&R2: CMBs detected by both rater 1 and 2. R1, R2: CMBs detected exclusively by rater 1 or by rater 2. C: additional CMBs detected at consensus meeting.

[b] Total of detected locations; divided in true positives (TP), extra positives (EP), and false positives (FP). Extra positives were CMBs detected by the RST, but not during the initial visual rating.

[c] Final total combining visual total (VT) and extra positives (EP), together with the false negatives (FN).

Table 2: Sensitivity of the individual raters, both raters combined, and the automatic detection. A total of 66 microbleeds was present in the images.

	#TP	#FP	#FN	Sensitivity
Rater 1	34	4	32	51.5 %
Rater 2	44	18	22	66.7 %
Rater 1+2	53	0	13	80.3 %
Automatic	47	309	19	71.2 %

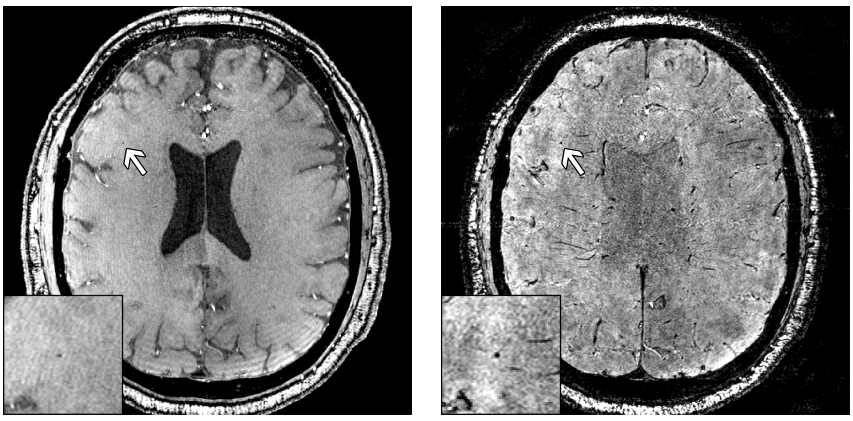

(a) First echo (b) Second echo

Figure 5: A typical microbleed that is detected by the RST.

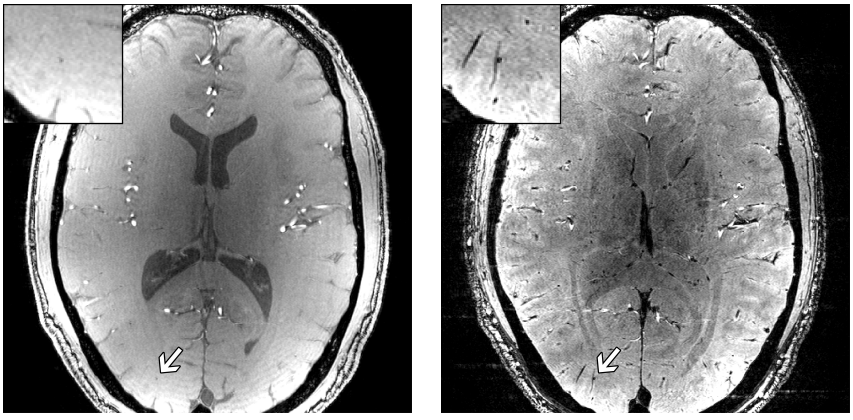

(a) First echo (b) Second echo

Figure 6: A microbleed detected by the RST, where the microbleed is adjacent to a vessel.

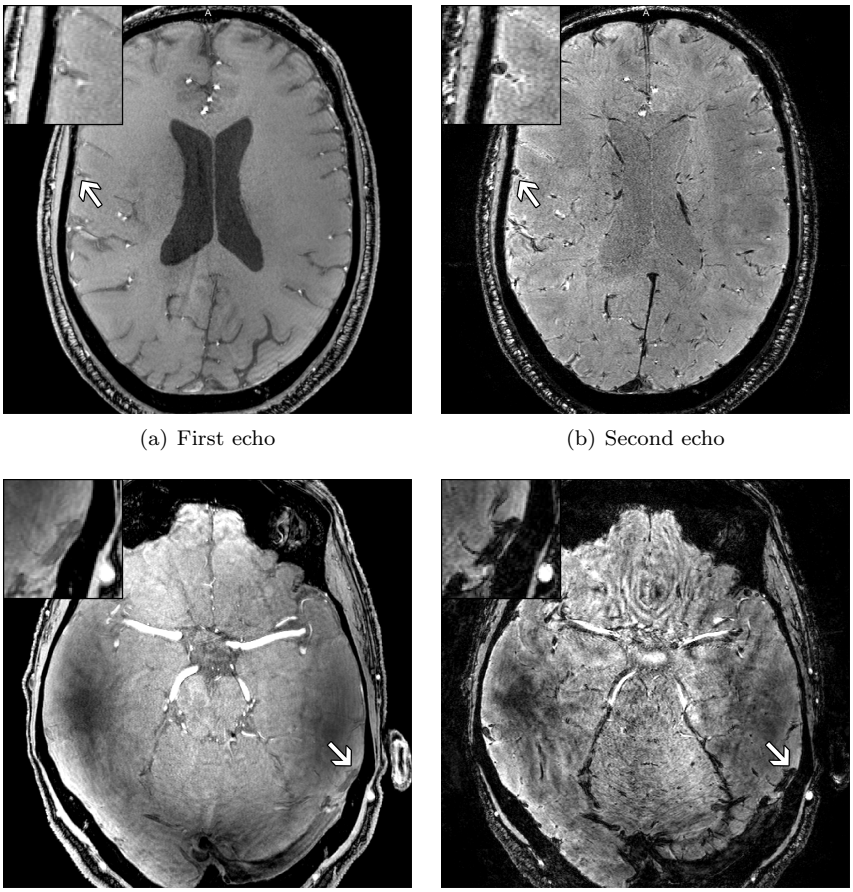

(a) First echo (b) Second echo

(c) First echo (d) Second echo

Figure 7: Two typical false positives, in two different participants, that were detected by the RST as microbleeds. Both involved large blood vessels, where false positives typically occur at curved sites within the vessel.

vessel. Since there is still enough radial symmetry contribution from the sides of the CMB that are not touching the vessel, detection is not a problem for the RST. False positives were mainly caused by large blood vessels, as shown in Figure 7. The anatomical nature of vessels can sometimes generate significant radial symmetry contribution at highly curved regions to be detected by the RST as a CMB, especially with large vessels that have many contributing gradients on the surface. Figure 8 shows a typical false negative caused by the microbleed not being visible on the first echo time image.

4 Discussion

Detection of cerebral microbleeds can be achieved by the radial symmetry transform on 7.0 T MRI scans, with a high sensitivity and a limited number of false positives. The semi-automatic method showed a large reduction in rating

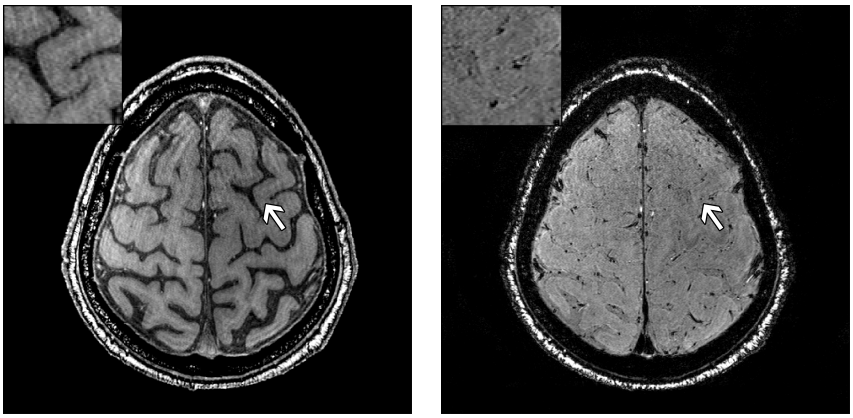

(a) First echo (b) Second echo

Figure 8: A typical false negative, where the microbleed is not visible on the first echo.

time: from 30 to 2 min per participant. Most importantly, the method outperformed individual raters in terms of sensitivity and even detected microbleeds that were missed in the visual rating.

We tried to optimize human rating so as to arrive at a reliable reference standard. However, this was only successful to a limited extent, because of the fundamental problems that arise during microbleed rating on high-resolution 7.0 T MR images. 7.0 T MR imaging is known to have a higher sensitivity for microbleed detection than scans acquired at lower field strength (Conijn et al. 2011). However, the limited size of some of the lesions and susceptibility effects of adjacent other structures complicates detection, which leads to a modest sensitivity of the visual rating on 7.0 T MRI scans (de Bresser et al. 2013). The described sensitivities of raters 1 and 2 are in line with sensitivities reported by De Bresser et al., who found a mean sensitivity of 60 % (range: 44 to 83 %). De Bresser et al. also reports higher sensitivities of the same raters when performing visual rating on 1.5 T MR scans, which indicates that the reduced sensitivity is caused by the increased difficulty in rating at 7.0 T MR scans.

Visual rating of CMBs on 7.0 T MR images will not result in a ground truth rating that can be considered as a golden standard, but rather as a "silver" standard. The original visual rating was combined with the extra positives detected by the RST to construct a ground truth rating with maximum sensitivity, even though this will introduce a bias in the sensitivities in favour of the RST. The extra positives were confirmed as true microbleeds by two raters independently. Visual rating by human raters can not guarantee that 100 % of all present CMBs have been detected, thus adding CMBs found by other means to the ground truth rating will improve the ground truth.

Nineteen microbleeds that were detected by the initial human raters were missed by the RST. Of these false negatives, 7 were not visible on the first echo and 4 were not visible on the second echo, which was a prerequisite for our variant of the RST to detect CMBs. The microbleeds that were not visible on

the first echo were either completely absent or too small in size to have any response to the used Sobel kernel. Their mean diameter on the second echo, in which CMBs appear larger than on the first echo owing to the blooming effect, was 0.78 ± 0.18 mm. This makes it difficult for human raters to detect those microbleeds and in most other studies such small microbleeds were even ignored (as indicated in the review study by Cordonnier et al. (2007)). The microbleeds that were invisible on the second echo disappeared in the blooming effect, caused by vessels nearby, and had a radial symmetry value far above the threshold θ_2. Work by Conijn et al. (2010) showed that 15.4 % of microbleeds were not visible on the first echo and 1.9 % were not visible on the second echo. As the missing microbleeds on the second echo were relatively large and thus had a radial symmetry value far below the threshold θ_1 on the first echo, there should be a possibility to detect them. This will be investigated in future work.

The remaining eight false negatives were caused by various problems. Artefacts visible in one T2*-weighted image (acquired in 2008) caused some false negatives. Advances in the quality of 7.0 T MR imaging might improve this in the future. In the remaining cases, there was not enough contribution of the microbleeds to the radial symmetry in order to be detectable. A total of 7 false negatives were scored as possible microbleeds by raters 1 and 2, indicating that they were not sure about the lesion being a definite microbleed or something else. The lack of radial symmetry at these locations might possibly indicate that these lesions were not microbleeds and should have been ignored.

During preprocessing, a binary mask of the grey and white matter was created using SPM8, but another segmentation method can be used as well. Completely removing all cerebrospinal fluid by setting a lower-threshold of 90 % on the probability-mask produced by SPM8 is required to reduce the number of false positives. The sulci present in the brain can have a large radial symmetry value, especially in the far end of a sulcus, resulting in false positives.

Computation time of the RST was about one hour per participant, using one core of a standard workstation. However, the computation of the radial symmetry contribution of multiple radii could be parallelized, which e.g. would reduce the computation time to 15 min on a typical quad-core workstation.

The RST performs excellently in terms of sensitivity and false positives, in comparison with the other two semi-automated CMB detection methods published so far, by Seghier et al. (2011) and Barnes et al. (2011). Our study and these previous studies clearly differ in MR acquisition protocols and field strengths. Nevertheless, the method described by Seghier et al. identified 77 % of all patients, while the RST identified 94 % of the participants. The participant that was not identified by the RST had a single microbleed that was rated 'possible' and not 'definite' by the human raters. As numbers on false positives were not provided, only the time required to remove the false positives could be compared. The method of Seghier et al. required on average 5 to 10 min time to remove the false positives, compared to 1.5 to 2.5 min for the RST, which is likely due to a high number of false positives in the method of Seghier et al. The method described by Barnes et al. had a sensitivity of 81.7 %, which is higher compared to the sensitivity of 71.2 % for the RST. However, the reported number of false positives in the method of Barnes et al. is much higher: on average 107.5 per patient compared to 17.2 per participant for the RST. This explains the longer rating time required after processing for the method of Barnes et al. The higher sensitivity might be explained by the differences

in size of the microbleeds found in the patients of Barnes and the participants in this study. Although not precisely specified, Barnes et al. reported microbleed sizes of <5 to 10 mm. In this study, the microbleeds visible on the first echo of the used T2*-weighted MR scan range from 0.3 to 2.0 mm and seven microbleeds were not visible at all. Since the RST does not produce many false negatives on larger microbleeds, this method might perform better when searching only for larger microbleeds. The latter was commonly done in most studies (Cordonnier et al. 2007).

Applying the RST to an anisotropic scan acquired at lower field strength is also possible. The individual components of the gradient direction are scaled with the voxel size, to account for anisotropic voxels. However, the voxel size gives rise to a lower limit on the detection of CMBs, since it is not possible to detect CMBs of only one or a few voxels in size. There would hardly be any radial symmetry contribution for microbleeds that consist of so few voxels. This could be counteracted by adapting the thresholds, which can result in additional false positives and more censor-time afterwards, or increasing the echo time, resulting in a larger apparent size of the CMBs. With an increase in apparent size, CMBs could consist of more voxels and might be detectable by the RST.

The RST outperforms individual human raters in terms of sensitivity and required human rater time. Combining the rating of two individual raters in a consensus meeting will result in the highest sensitivity, but still not 100 %, and takes even more time. This indicates the difficulty in the manual rating of cerebral microbleeds in high-resolution MR scans. In daily practice, a scan is usually rated by a single rater, since time constraints do not permit multiple raters and a consensus meeting. Semi-automatic detection of microbleeds with the RST will decrease rating time and increase the sensitivity significantly.

5 Conclusion

The radial symmetry transform can be used to detect cerebral microbleeds on high-resolution, nearly isotropic brain MR scans with a high sensitivity. Removing the false positives requires 2 min by an experienced rater, as compared with 30 min for full visual rating of the cerebral microbleeds.

6 Acknowledgments

This work was financially supported by the project Care4Me (Cooperative Advanced REsearch for Medical Efficiency) in the framework of the EU research program ITEA (Information Technology for European Advancement). The authors thank Drs. Jaco J.M. Zwanenburg, Theo D. Witkamp, Taro Takahara, and Manon Brundel for assisting in the data acquisition and analysis.

References

Ashburner, J. and K. J. Friston (2005). "Unified segmentation". In: *NeuroImage* 26, pp. 839–851.

Barnes, S. R. S. et al. (2011). "Semiautomated detection of cerebral microbleeds in magnetic resonance images". In: *Magnetic Resonance Imaging* 29.6, pp. 844–852.

Bresser, J. de et al. (2013). "Visual Cerebral Microbleed Detection on 7T MR Imaging: Reliability and Effects of Image Processing". In: *American Journal of Neuroradiology* 34.6, E61–E64.

Conijn, M. M. A. et al. (2010). "Visualization of cerebral microbleeds with dual-echo T2*-weighted magnetic resonance imaging at 7.0 T". In: *Journal of Magnetic Resonance Imaging* 32.1, pp. 52–59.

Conijn, M. M. A. et al. (2011). "Cerebral Microbleeds on MR Imaging: Comparison between 1.5 and 7T". In: *AJNR Am J Neuroradiol* 32.6, pp. 1043–1049.

Cordonnier, C., R. A.-S. Salman and J. M. Wardlaw (2007). "Spontaneous brain microbleeds: systematic review, subgroup analyses and standards for study design and reporting". In: *Brain* 130.8, pp. 1988–2003.

De Reuck, J. et al. (2011). "Comparison of 7.0 T T2*-Magnetic Resonance Imaging of Cerebral Bleeds in Post-Mortem Brain Sections of Alzheimer Patients with Their Neuropathological Correlates". In: *Cerebrovasc Dis* 31.5, pp. 511–517.

Fazekas, F. et al. (1999). "Histopathologic Analysis of Foci of Signal Loss on Gradient-Echo T2*-Weighted MR Images in Patients with Spontaneous Intracerebral Hemorrhage: Evidence of Microangiopathy-Related Microbleeds". In: *American Journal of Neuroradiology* 20, pp. 637–642.

Greenberg, S. M. et al. (2009). "Cerebral microbleeds: a guide to detection and interpretation". In: *The Lancet Neurology* 8.2, pp. 165–174.

Gregoire, S. M. et al. (2009). "The Microbleed Anatomical Rating Scale (MARS): Reliability of a tool to map brain microbleeds". In: *Neurology* 73.21, pp. 1759–1766.

Knudsen, K. A. et al. (2001). "Clinical diagnosis of cerebral amyloid angiopathy: Validation of the Boston Criteria". In: *Neurology* 56.4, pp. 537–539.

Kuijf, H. J. et al. (2011). "Detecting cerebral microbleeds in 7.0 T MR images using the radial symmetry transform". In: *IEEE International Symposium on Biomedical Imaging: From Nano to Macro*, pp. 758–761.

Loy, G. and A. Zelinsky (2003). "Fast radial symmetry for detecting points of interest". In: *IEEE Transactions on Pattern Analysis and Machine Intelligence* 25.8, pp. 959–973.

McAuley, G. et al. (2011). "Iron quantification of microbleeds in postmortem brain". In: *Magnetic Resonance in Medicine* 65.6, pp. 1592–1601.

Seghier, M. L. et al. (2011). "Microbleed Detection Using Automated Segmentation (MIDAS): A New Method Applicable to Standard Clinical MR Images". In: *PLoS ONE* 6.3, e17547.

Simons, P. et al. (1999). "Second Manifestations of ARTerial disease (SMART) study: Rationale and design". In: *European Journal of Epidemiology* 15 (9), pp. 773–781.

Theysohn, J. M. et al. (2011). "7 tesla MRI of microbleeds and white matter lesions as seen in vascular dementia". In: *Journal of Magnetic Resonance Imaging* 33.4, pp. 782–791.

Vernooij, M. W. et al. (2008). "Prevalence and risk factors of cerebral microbleeds: The Rotterdam Scan Study". In: *Neurology* 70.14, pp. 1208–1214.

Wardlaw, J. M. et al. (2006). "Cerebral Microbleeds Are Associated With Lacunar Stroke Defined Clinically and Radiologically, Independently of White Matter Lesions". In: *Stroke* 37.10, pp. 2633–2636.